TEMPORAL AND SPATIAL DISTRIBUTION OF REFERENCE CROP EVAPOTRANSPIRATION IN NORTH CHINA PLAIN

JIN, X. D.[1,4] – ZHAO, Z.[1,2,4] – ZHANG, L.[3,5*] – ZHAO, G. F.[2] – LIU, X.[1,4] – ZHENG, Z.[1,4]

[1]*Henan Yellow River Engineering Consulting Co., Ltd, Zhengzhou 450003, China*

[2]*Economic Development Administration of Henan Yellow River Bureau, Zhengzhou 450003, China*

[3]*North China University of Water Resources and Electric Power, Zhengzhou 450046, China*

[4]*Henan Engineering Research Center for Protection and Governance of Yellow River, Zhengzhou 450003, China*

[5]*Department of Geography and Environmental Management, University of Waterloo, 200 University Avenue West, Waterloo, Ontario N2L 3G1, Canada*

**Corresponding author*
e-mail: zhanglei@ncwu.edu.cn

(Received 19th Jun 2023; accepted 9th Feb 2024)

Abstract. Reference evapotranspiration (ETo) is the main influencing factor of crop water balance. Based on data from 170 meteorological stations in the North China Plain (NCP) from 1970 to 2019, moving average method, Mann-Kendall test, improved ordered cluster analysis, inverse distance weighted interpolation (IDW), ordinary least squares regression (OLS), geographically weighted regression (GWR) and hotspot analysis, were used to analyze the spatial and temporal variation of ETo in NCP. The ETo in NCP showed a significant decreasing trend with 99% confidence. The high ETo value range (1085~1039 mm/year) appears in the west and south of Bohai Bay. The northern part of the Bohai Bay witnessed relatively low ETo value (909~997 mm/year). It is qualitatively judged that wind speed is the main factor affecting ETo in NCP. Results by the GWR model further confirm that wind speed was the dominant factor affecting ETo in NCP. Based on the hotspot analysis, it was found that the hot spots shrank sharply, and the hot spots were more likely to become areas with high ETo values over time. Results of this study can help in better understanding the spatial and temporal distribution of regional ETo in NCP and allocation of agricultural water resources.
Keywords: *reference evapotranspiration, North China Plain, correlation, space-time variation, high-quality development, Yellow River Basin*

Introduction

In general, crop coefficient method and Reference evapotranspiration (ETo) can be used to estimate crop water requirements (Jensen Marvin and Haise Howard, 1963; Priestley and Taylor, 1972; Turc, 1961; Ge et al., 2022; Zhao et al., 2023). ETo is a hypothetical evapotranspiration of standard reference crops (The reference crop is an idealized crop representing a specific land surface, commonly exemplified by crops such as alfalfa, tall fescue, and grass.) under established standards. Its accuracy directly affects the water quantity simulation in the process of crop growth, and thus has an important impact on the prediction, planning and allocation of agricultural water use in a large range (George, 1975).

In real life, it is also a major concern of managers to refer to the temporal and spatial distribution variation of crop evapotranspiration and its main meteorological factors. Timely updating of regional reference crop evapotranspiration rules is helpful for managers to adjust water use plans for hot spots and maximize target benefits. Many

http://www.aloki.hu ● ISSN 1589 1623 (Print) ● ISSN 1785 0037 (Online)
DOI: http://dx.doi.org/10.15666/aeer/2302_18971921

scholars in China and abroad have used a variety of research methods to study the relevant spatio-temporal laws (Zhang et al., 2022b). Bandyopadhyay et al. (2009) analyzed the meteorological data of 133 stations in India from 1971 to 2002 and calculated the corresponding reference crop evapotranspiration. The results reflected the significant reduction trend of reference crop evapotranspiration was caused by the decrease of wind speed and the increase of relative humidity. This conclusion was echoed by Srivastava et al.'s (2010) study of cities such as Hyderabad, India, where wind speed was the main factor affecting reference crop evapotranspiration. In a considerable part of Iran, Dinpashoh et al. (2011) found that wind speed was still the dominant factor for reference crop evapotranspiration (except in winters). The research of Tabari et al. (2012) showed that reference crop evapotranspiration at the seasonal and monthly scales in Iran had a significant increasing trend. Pour et al. (2020) evaluated reference crop evapotranspiration and its factors in Peninsular Malaysia and found an increasing trend in reference crop evapotranspiration, with an increase in minimum temperature considered to be the main driver of this trend.

In China, Hao et al. (2013) studied the changes in parts of the Huaihe River Basin from 1959 to 2009, and found that the decrease of wind speed and radiation was the reason for the decline of reference crop evapotranspiration in the region. Zhang et al. studied the changes in the Loess Plateau during 1961-2010, and found that the increase of average temperature was the most important factor for the significant increase of reference crop evapotranspiration in this region. At the same time, lower solar radiation and wind speed play a secondary role (Bo and TiaoFeng, 2013). Duan et al. (2015) studied the situation around Nantong from 1961 to 2011, and found that the evapotranspiration of reference crops in this region did not change significantly, but precipitation and relative humidity were significantly negatively correlating factors. Li et al. (2017) studied the Fenhe irrigation area from 1951 to 2014, and the results indicated that the change of reference crop evapotranspiration in this area was not obvious. In terms of annual variation, the main affecting factors in the irrigated area were temperature, relative humidity and wind speed during the period of April and June, and sunshine duration from May to September. Zhang et al. (2019) studied the relevant changes throughout China during 1970-2014, and found that maximum temperature, relative humidity and wind speed were the main climate variables affecting reference crop evapotranspiration based on least square regression, and maximum temperature and minimum temperature were the climate variables with the greatest influence based on geographically weighted regression.

The above results clearly indicate, with the development and changes in a long period of time in the past, the reference evapotranspiration of crops in different regions of the world also changes with the change of climate, but the main reasons for the change in each region are often different. Although there are numerous studies on the spatio-temporal distribution of reference crop evapotranspiration, it is easier to judge the significance of reference crop evapotranspiration in spatial distribution and clustering than the significance of the time trend. Based on this, this paper will introduce a hot spot analysis technique to identify the significance of spatial distribution. Optimized hot spot analysis (Zhang et al., 2019) is a new geostatistics method. It uses Gi* (Getis-Ord) statistics to identify the localized hot spots and cold spots along with their statistical significance in spatial characteristics, so as to obtain hot spot map and cold spot map. Optimization hotspot analysis has been widely used in many fields, such as criminology research (Craglia et al., 2000), emergency

http://www.aloki.hu ● ISSN 1589 1623 (Print) ● ISSN 1785 0037 (Online)
DOI: http://dx.doi.org/10.15666/aeer/2302_18971921

management (Songchitruksa and Zeng, 2010), heat vulnerability assessment (Wolf and McGregor, 2013), natural disaster assessment (Gajović and Todorovic, 2013). However, it has not been tried in the study of spatial distribution of reference evapotranspiration. In this paper, the applicability of optimized hot spot analysis to reference crop evapotranspiration spatial characteristics is discussed. On this basis, the distribution characteristics of hot spot and cold spot were discussed, and the influence mechanism of spatial scale and meteorological factors on hot spot and cold spot was revealed, providing theoretical support for further improvement of spatial scale of water demand information.

As an important agricultural crop base in China, it is necessary to make accurate water resources management in North China Plain according to the temporal and spatial distribution of ETo and its variation trend. Therefore, this study will make a systematic evaluation of the temporal and spatial distribution characteristics of ETo based on the current meteorological data of the latest period. The research focuses on: (1) Using five-point moving average method, Mann-Kendall test and other methods to judge the interannual trend change of ETo; (2) Spatial variability of ETo and meteorological elements was analyzed based on GIS and spatial interpolation techniques; (3) Investigating the applicability of ordinary least square regression and geographically weighted regression, and analyzing the sensitivity and spatial relationship between ETo and various meteorological factors; (4) Getis-Ord statistics was used to analyze hot and cold spots to evaluate the statistical significance of the spatial variation of ETo, so as to find the statistical significance between different months and years.

Data and methods

Study area

The North China Plain is one of the three great plains in China. It starts from the Yanshan Mountains in northern area, reaching the Yellow River in the south, bordering the Bohai Sea in the east and the Taihang Mountains in the west. The geographical coordinates are located between 34°46’–40°25’ north latitude and 112°30’–119°30’ east longitude. The total area is about 139,200 km^2. As a whole, it covers the whole plain of Beijing, Tianjin, Hebei Province, and the plain north of the Yellow River within the boundaries of Henan and Shandong provinces. The plain is a warm temperate semi-arid monsoon climate zone on the east coast of Eurasia continent. It is windy in spring, hot and rainy in summer, sunny and cool in autumn, cold and dry in winter, with four distinct seasons. The average annual precipitation is 556.48 mm. The distribution of precipitation within the year is very uneven, mainly concentrated in July to September, accounting for about 75% of the total annual precipitation, the least winter, easy spring early autumn waterlogging, late autumn and drought. The average annual temperature ranges from 10℃ to 14℃, with the lowest temperature in January ranging from -1.8℃ to 1.0℃, and the highest temperature in July ranging from 26℃ to 32℃. The annual average sunshine duration is between 6~8 h, and the frost-free period is more than 200 days. The evaporation of water surface is between 1100~2000 mm. The wind speed near the ground is between 1.5 and 3.5 m/s. The study area is an important agricultural base and acts as the main grain and cotton sources in China, with the grain sown area accounting for more than 80% of the total crop sown area in the region. It is an agricultural area dominated by dry farming, and the north of the Yellow River is dominated by three crops in two years. In most areas south of the Yellow River, there

http://www.aloki.hu ● ISSN 1589 1623 (Print) ● ISSN 1785 0037 (Online)
DOI: http://dx.doi.org/10.15666/aeer/2302_18971921

are two crops a year, three crops in two years and five crops in three years. The multiple cropping index ranks first in North China. Wheat and corn are the main food crops in North China, and the main cash crops are flue-cured tobacco, sesame, cotton, soybean and so on (He et al., 2022; Koch et al., 2020; Yang, Li, Wang and Wang, 2022; Zhang et al., 2022a; Zhang et al., 2022c). In this paper, 170 national meteorological stations within the study area are investigated. And *Figure 1* gives their locations.

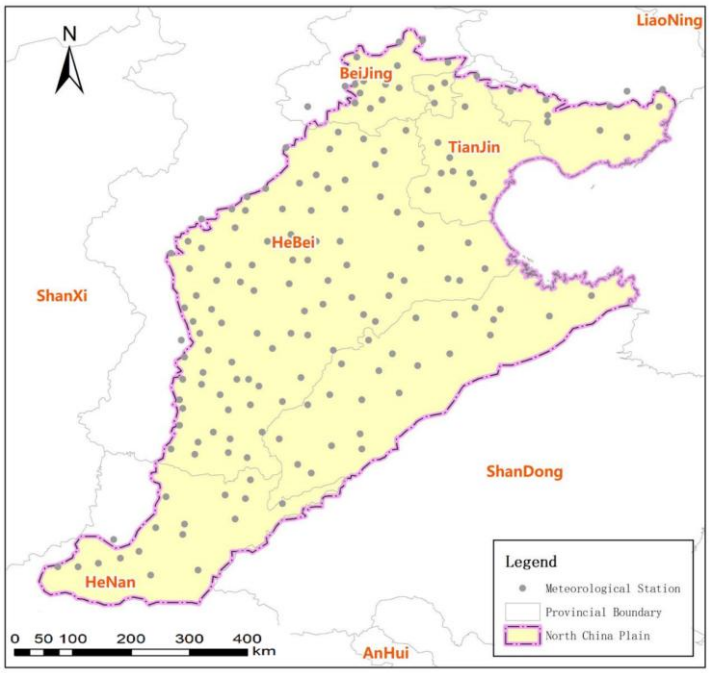

Figure 1. *Distribution map of meteorological stations in North China Plain*

Data sources and characteristics

Meteorological data of 170 stations from 1970 to 2019 were collected from http://data.cma.gov.cn, including precipitation (*P*), relative humidity (*RH*), sunshine duration (*SH*), wind speed (*WS*) at 2 m height, average temperature (T_{mean}), maximum temperature (T_{max}) and minimum temperature (T_{min}). *Table 1* summarizes the mean values and standard deviations of the aforementioned meteorological elements and ETo at each station. Among them, the ETo value adopted is calculated from meteorological data according to the FAO-Penman-Monteith formula.

Table 1. *Statistics of meteorological factors (1970–2019)*

Factor	*P* (mm)	*RH* (%)	*SH* (h)	*WS* (m/s)	T_{mean} (°C)	T_{max} (°C)	T_{min} (°C)	*ETo* (mm/y)
Average value	539	64	2432	2.28	13	18.9	7.9	1036.3
Standard deviation	46.26	3.35	155.32	0.37	0.76	0.76	0.9	46.93

Precipitation (P), relative humidity (RH), sunshine duration (SH), wind speed (WS) at 2 m height, average temperature (Tmean), maximum temperature (Tmax) and minimum temperature (Tmin). Reference evapotranspiration (ETo)

http://www.aloki.hu ● ISSN 1589 1623 (Print) ● ISSN 1785 0037 (Online)
DOI: http://dx.doi.org/10.15666/aeer/2302_18971921

Methods

FAO-Penman-Monteith method

The FAO-Penman-Monteith (FAO-PM) method is based on basic physics and uses energy and mass balance to calculate ETo, which gives it a high degree of universality (Allan et al., 1998). However, the method requires too many meteorological elements, which limits its application in areas lacking meteorological elements (Liu et al., 2020; Zhang et al., 2018; Zhang et al., 2023). Its basic formula is:

$$ETo_{PM} = \frac{0.408\Delta\left(R_n - G\right) + \gamma \frac{900}{T+273} U_2 \left(e_s - e_a\right)}{\Delta + \gamma\left(1 + 0.34U_2\right)} \quad \text{(Eq.1)}$$

where, ETo_{PM} is the calculated reference crop evapotranspiration, $\mathrm{mm \cdot d^{-1}}$; e_s and e_a are saturation and actual vapor pressure respectively, kPa; Δ is the slope of the relation curve between saturated water vapor pressure and air temperature, $\mathrm{kPa \cdot ℃^{-1}}$; γ is hygrometer constant, $\mathrm{kPa \cdot ℃^{-1}}$; U_2 is wind speed 2 m above the ground, $\mathrm{m \cdot s^{-1}}$; T is the average daily temperature 2 m above the ground, ℃; G is soil heat flux, and its value is 0, $\mathrm{MJ \cdot m^{-2} \cdot day^{-1}}$; R_n is the net radiation on the crop surface (Allan et al., 1998), $\mathrm{MJ \cdot m^{-2} \cdot day^{-1}}$.

U_2 is calculated as:

$$U_2 = U_z \frac{4.87}{\ln\left(67.8z - 5.42\right)} \quad \text{(Eq.2)}$$

where: U_z is the wind speed at z m above the surface, $\mathrm{m \cdot s^{-1}}$. In this paper the wind speed is obtained at 10 m above the ground, so $z = 10\mathrm{m}$.

Trend analysis

Over time, ETo sequences in specific regions may show a certain trend of change, which is reflected in the positive correlation between ETo and year (increasing trend) or negative correlation between ETO and year (decreasing trend). Referring to other trend test methods for hydrological series, this paper uses five-point moving average method (Lv et al., 2013) to identify the change trend of ETo, and then uses Spearman rank correlation test to judge the significance of such trend.

(1) Five-point sliding average method: for a certain time sequence X = (x1, x2... , xn), the five-point moving average method calculates the average value by determining the pre and post values of the sequence values to get a new sequence Y = (y1, y2... , yn-4) to show the changing trend. This transformation relationship can be expressed as follows:

$$y_t = \frac{\sum_{i=-2}^{2} x_{t+2+i}}{5}, t = 1,2,\ldots,n-4 \quad \text{(Eq.3)}$$

(2) Spearman rank correlation test: This method uses the correlation between ETo sequence and year sequence and the following statistic T is established:

http://www.aloki.hu ● ISSN 1589 1623 (Print) ● ISSN 1785 0037 (Online)
DOI: http://dx.doi.org/10.15666/aeer/2302_18971921

$$T = r_s \sqrt{\frac{n-2}{1-r_s^2}} \square t(n-2) \quad \text{(Eq.4)}$$

where, n represents sample number; t (n-2) represents the T-distribution with n-2 freedom degrees; r_s refers to Spearman rank correlation coefficient, which can be calculated as follows:

$$r_s = 1 - \frac{6\sum_{i=1}^{n}(R_i - Q_i)^2}{n(n^2-1)} \quad \text{(Eq.5)}$$

In the above formula, Ri and Qi refer to the rank of the year and ETo sample respectively.

Mutation diagnosis

Mann-Kendall test method constructs the following sequence (Zhang et al., 2020):

$$s_k = \sum_{i=1}^{k} r_i,\ k = 2,3,...,n \quad \text{(Eq.6)}$$

where, $r_i = \begin{cases} 1 & x_i > x_j \\ 0 & \text{other} \end{cases}$, $j = 1,2,...,i$.

Define the statistic UF_k:

$$UF_k = \frac{\left[s_k - E(s_k)\right]}{\sqrt{Var(s_k)}},\ k = 1,2,...,n \quad \text{(Eq.7)}$$

where, $E(s_k) = n(n+1)/4$, $Var(s_k) = n(n-1)(2n+5)/72$, and $UF_1 = 0$. In reverse order, repeat the process, and obtain $UB_k = -UF_k$, in which $k = n, n-1,\ldots,1$, and $UB_1 = 0$.

Improved ordered cluster analysis method, and try to apply it to the judgment of ETo mutation. The objective function of traditional ordered clustering analysis to seek mutation points is to minimize the sum of squares of the deviations between the same species, while Yuan Man et al. believe that the principle of small deviations between the same species and large deviations between classes should be considered at the same time (Yuan et al., 2017). The deviation between different classes can be expressed as:

$$d = \left|\overline{x}_t - \overline{x}_{n-t}\right| \quad \text{(Eq.8)}$$

where, $\overline{x}_t$ and $\overline{x}_{n-t}$ are the mean values of the two sequences before and after time t respectively. The difference between the same species can be written as:

http://www.aloki.hu ● ISSN 1589 1623 (Print) ● ISSN 1785 0037 (Online)
DOI: http://dx.doi.org/10.15666/aeer/2302_18971921

$$\sigma_t = \sqrt{\sum_{i=1}^{t}\left(x_i - \overline{x}_t\right)^2 \Big/ t} \quad \text{(Eq.9)}$$

$$\sigma_{n-t} = \sqrt{\sum_{i=t+1}^{n}\left(x_i - \overline{x}_{n-t}\right)^2 \Big/ \left(n-t\right)} \quad \text{(Eq.10)}$$

Therefore, the objective function constructed by the improved ordered cluster analysis is as follows:

$$\min S(t) = \min\left(\sigma_t + \sigma_{n-t} - d\right) \quad \text{(Eq.11)}$$

Inverse distance-weighted interpolation

Inverse distance weighting, also known as inverse distance power, is a deterministic interpolation method based on the near similarity principle. The inverse distance weighting method can be used for accurate or smooth interpolation. The power parameter controls that the weight coefficient decreases as the distance from a grid node increases. For larger powers, points that are closer together are given higher weights; When given a smaller power, the weight of each interpolation point is evenly distributed. In particular, when the power is 1, it is called linear interpolation. The sum of all assigned weights should be equal 1 in a specific grid node. When the observation point coincides with the grid node, the observation point is given a full weight of 1, that is, it is an accurate interpolation. Inverse distance weighting can be expressed as:

$$T_{i,j} = \sum_{k=1}^{n} T_k d_k^{-2} \Big/ \sum_{k=1}^{n} d_k^{-2} \quad \text{(Eq.12)}$$

where, $T_{i,j}$ are the element values of grid points to be interpolated; n is the number of sites referenced to the interpolation point; T_k is the factor value of the kTH point; k is the number of referenced interpolation points; d_k^{-2} is the reciprocal of the square distance between the kTH point and the point to be interpolated.

In addition, a typical defect of the inverse distance-weighted interpolation method is that it is easy to produce the phenomenon of "bull's eye" around the observation point, which can be alleviated by setting smooth parameters. That is, for a specific node, no matter whether the observation point is coincident with the node or not, the observation point with full weight assignment should be avoided.

Ordinary least squares regression

Ordinary least square regression (OLS) is a parameter estimation using all available observational data, which is essentially a global estimation and grasp. OLS expects the sum of residual squares of all observations to reach the minimum, and believes that observation data at different spatial locations of samples do not interact with each other. The sample matrix X is composed of m n-dimensional samples, and the parameter matrix β is to be obtained:

http://www.aloki.hu ● ISSN 1589 1623 (Print) ● ISSN 1785 0037 (Online)
DOI: http://dx.doi.org/10.15666/aeer/2302_18971921

$$X = \begin{bmatrix} 1 & x_1^{(1)} & \cdots & x_n^{(1)} \\ 1 & x_1^{(2)} & \cdots & x_n^{(2)} \\ \vdots & \vdots & \vdots & \vdots \\ 1 & x_1^{(m)} & \cdots & x_n^{(m)} \end{bmatrix} \quad \text{(Eq.13)}$$

$$\beta = \begin{bmatrix} \beta_0 & \beta_1 & \cdots & \beta_n \end{bmatrix}^T \quad \text{(Eq.14)}$$

The object function of OLS is:

$$O(\beta) = \frac{1}{2}(X\beta - Y)^T (X\beta - Y) \quad \text{(Eq.15)}$$

When X^TX is a full rank matrix or a positive definite matrix, the gradient can be obtained directly:

$$\nabla O(\beta) = X^T X\beta - X^T Y \quad \text{(Eq.16)}$$

Let $\nabla O(\beta) = 0$, therefore $\beta = (X^T X)^{-1} X^T Y$.

Geographically weighted regression

Geographic weighted regression (GWR) model further considers the spatial characteristics of data during the regression process. It is equivalent to the extension and expansion of the classical linear regression model, so that the regression variable parameters of basic spatial units can be estimated by local regression according to the subsample observation data information of adjacent spatial units. The form of GWR is:

$$y_i = \beta_0(u_i, v_i) + \sum_{j=1}^{k} \beta_{ij}(u_i, v_i) x_{ij} + \varepsilon_i \quad \text{(Eq.17)}$$

where, x_{ij} represents the *J*TH explanatory variable of the *i*ith spatial unit; y_i represents the interpreted variable of the *i*th spatial unit; (u_i, v_i) represents the geographical coordinates (latitude and longitude) of the *i*th spatial unit; β_{ij} (u_i, v_i) represents the *J*TH regression coefficient of the *i*th spatial unit, which is correlated with geographical coordinates. ε_i represents the random error of the *i*th space unit, which follows the normal distribution of 0 means and is independent of each other.

The selection of spatial weight matrix is the key to GWR model, showing important impact on the effectiveness of regression results. The following are some common spatial weight functions:

(1) Gaussian weight function:

$$w_{ij} = \Phi\left(\frac{d_{ij}}{\tau\theta}\right) \quad \text{(Eq.18)}$$

http://www.aloki.hu ● ISSN 1589 1623 (Print) ● ISSN 1785 0037 (Online)
DOI: http://dx.doi.org/10.15666/aeer/2302_18971921

where, d_{ij} represents the geographical distance between region i and region j; Φ represents the standard normal density function; τ represents the standard deviation of distance; θ represents the attenuation parameter.

(2) Exponential weight function:

$$w_{ij} = \sqrt{\exp(-\frac{d_{ij}}{\varphi})} \quad \text{(Eq.19)}$$

In the formula, φ represents the geographical distance between region i and the nearest neighbor region. The meanings of other parameters are the same as above.

(3) Cubic weight function:

$$w_{ij} = \left[1-\left(\frac{\theta}{d_{ij}}\right)^3\right]^3 \quad \text{(Eq.20)}$$

Hotspot analysis

The hot spot analysis in this paper is based on the G statistics of Getis-Ord to construct the map of hot spots and cold spots along with their statistical significance. The first step is to aggregate elements. Count Incidents Within Fishnet Polygons method is used to calculate the mean proximity distance and median proximity distance of meteorological stations, and adjust the pixel size according to this distance to get the fishnet surface grid. The second step is to analyze the scope of influence. If the range of influence is known, the known range of influence can be set to a fixed distance. If the influence range is unknown, Z-scores in statistics can be obtained with the help of Incremental Spatial Autocorrelation, and the distance corresponding to the peak Z-scores reflects the most significant distance of spatial clustering.

When there are multiple peaks, the distance corresponding to the first peak is used as the influence range. After the influence range is determined, let x_i and x_j be the values of ETo of meteorological stations i and j at various time scales, $w_{i,j}$ are the spatial weights of meteorological stations i and j, which can be understood as the influence of neighboring meteorological stations j on station i, and n is the total number of meteorological stations. According to *Equation 21*, G_i can be obtained:

$$G_i = \frac{\sum_{j=1}^{n} w_{i,j}x_j - \bar{X}\sum_{j=1}^{n} w_{i,j}}{S\sqrt{\frac{\left[n\sum_{j=1}^{n} w_{i,j}^2 - \left(\sum_{j=1}^{n} w_{i,j}\right)^2\right]}{n-1}}} \quad \text{(Eq.21)}$$

where, $\bar{X} = \sum_{j=1}^{n} x_j \Big/ n$, $S = \sqrt{\left(\sum_{j=1}^{n} x_j - \bar{X}^2\right)\Big/ n}$.

G_i statistics report standardized z and p values for each weather station. Higher z value and lower p value of a station could be identified a significant ETo hot spot.

http://www.aloki.hu ● ISSN 1589 1623 (Print) ● ISSN 1785 0037 (Online)
DOI: http://dx.doi.org/10.15666/aeer/2302_18971921

Negative z value and small p value could be defined as a significant ETo cold spot. In this paper, the Spatial Analysis Tool of ArcGIS 10.2 platform is used to analyze hot and cold spots.

Statistical Indicators

Two indicators including MAE and MRE, exactly the mean absolute error and mean relative error were utilized as objective indexes for model evaluation.

$$MAE = \frac{1}{n}\sum_{i=1}^{n}\left|ETo_{PM}(i) - ETo^{*}(i)\right| \quad \text{(Eq.22)}$$

$$MRE = \frac{1}{n}\sum_{i=1}^{n}\left|\frac{ETo_{PM}(i) - ETo^{*}(i)}{ETo_{PM}(i)}\right| \times 100\% \quad \text{(Eq.23)}$$

where, ETo_{PM} is the standard FAO-Penman-Monteith value, ETo* is the estimated value by the research model, and i is the index.

Results

Interannual situation of ETo

In this paper, the interannual variation of ETo sequence (total ETo value from 1970 to 2019) will be analyzed, and the research will be carried out from two aspects: the trend of change and the diagnosis of mutation. For trend analysis, five-point moving average method was used to judge the trend direction of ETo sequence, and Spearman rank correlation test helped judge the significance (*Table 2*). For the mutation diagnosis, the classical Mann-Kendall test and an improved ordered cluster analysis method were used to determine the mutation year range, and the run test method (Hu et al., 2014) could be used to judge the significance of the mutation.

Five-point sliding average processing was performed on yearly ETo series, and the ETo trend curve was drawn in *Figure 2*. Mann-Kendall test was performed for ETo sequences, with significance level $\alpha = 0.05$, and the results were in *Figure 3*. The intersection points of *UF* and *UB* was 1979, indicating that the change trend of ETo had a turning point in 1979.

Figure 4 shows the $S(t)$ curve of ETo. The relatively obvious low value appeared in 1983, and the improved ordered cluster analysis suggested that the ETo in North China Plain had an abrupt change in 1983. With the help of *Figure 3*, there is a high probability of mutation points around 1980, which requires significance level judgment.

Significance test of mutation year: This paper uses run test to determine significance of mutation point. According to the mutation year determined above, two ETo sequences of different lengths (n_1 and n_2) before and after the mutation year were labeled differently (0 and 1). It is assumed that the distribution functions of the sequences before and after the mutation are F_0 and F_1 respectively. The original hypothesis of the run test is $H0: F_0 = F_1$. In order to comprehensively investigate the influence of time periods, a total of 15 years from 1976 to 1990 of ETo sequence were respectively regarded as mutation years. SPSS software was used to conduct run test

http://www.aloki.hu ● ISSN 1589 1623 (Print) ● ISSN 1785 0037 (Online)
DOI: http://dx.doi.org/10.15666/aeer/2302_18971921

analysis on them, and the significance level of each year obtained was shown in *Figure 5*. With the significance level $\alpha = 0.01$, it can be seen that the years 1979 and 1983 can reject the null hypothesis, that is, $F_0 \neq F_1$. However, the significance level of 1981 is too high, and combined with the level of 1984-1987, this paper finally determined that 1983 is more reasonable as the ETo mutation year.

The moving average test, MK test and improved ordered cluster analysis were carried out for each meteorological element, as shown in *Figure 6*.

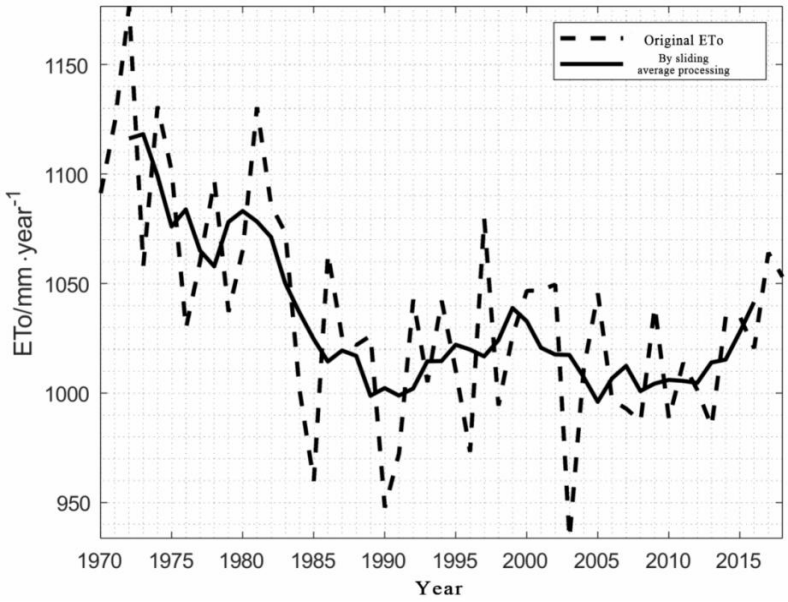

Figure 2. *Trend change curve of annual Eto*

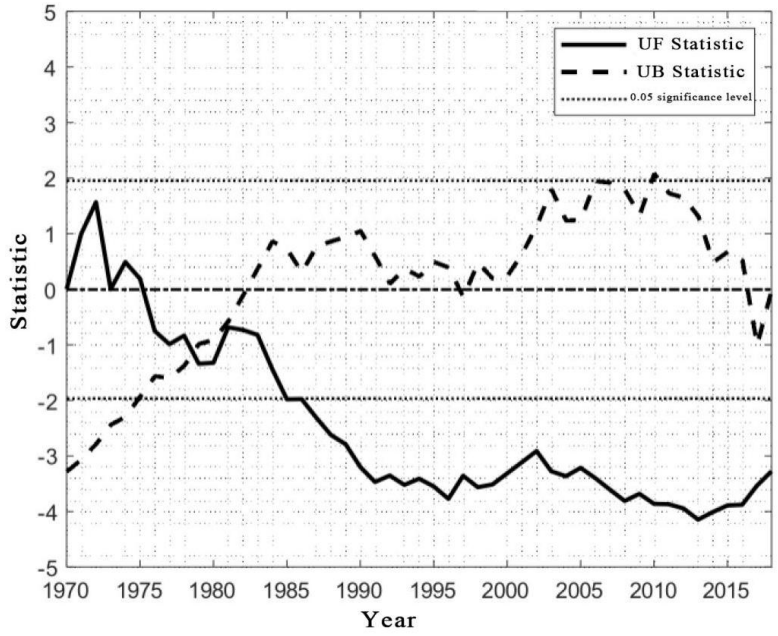

Figure 3. *Mann Kendall test statistics of annual ETo series*

http://www.aloki.hu ● ISSN 1589 1623 (Print) ● ISSN 1785 0037 (Online)
DOI: http://dx.doi.org/10.15666/aeer/2302_18971921

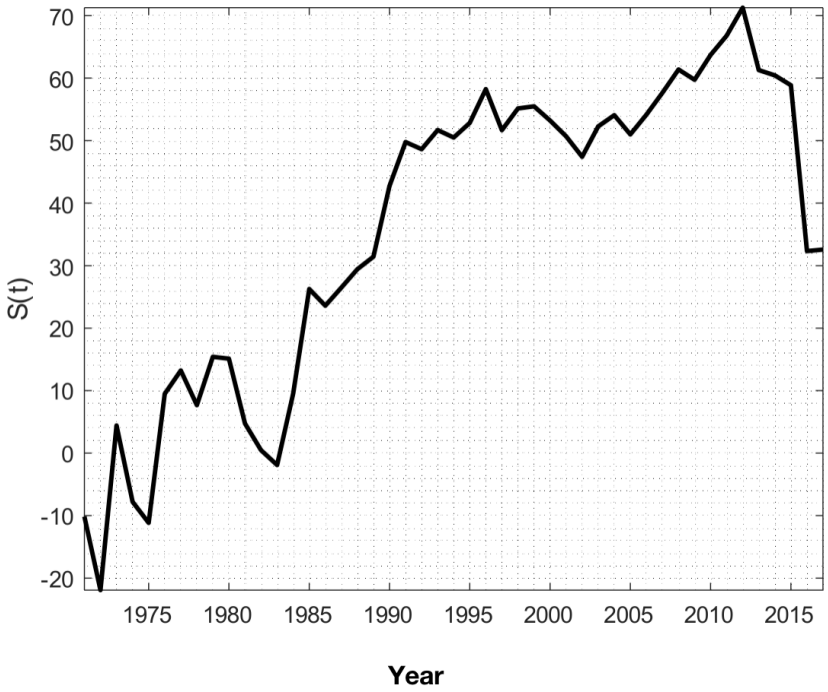

Figure 4. *S(t) via improved order cluster analysis of annual ETo series*

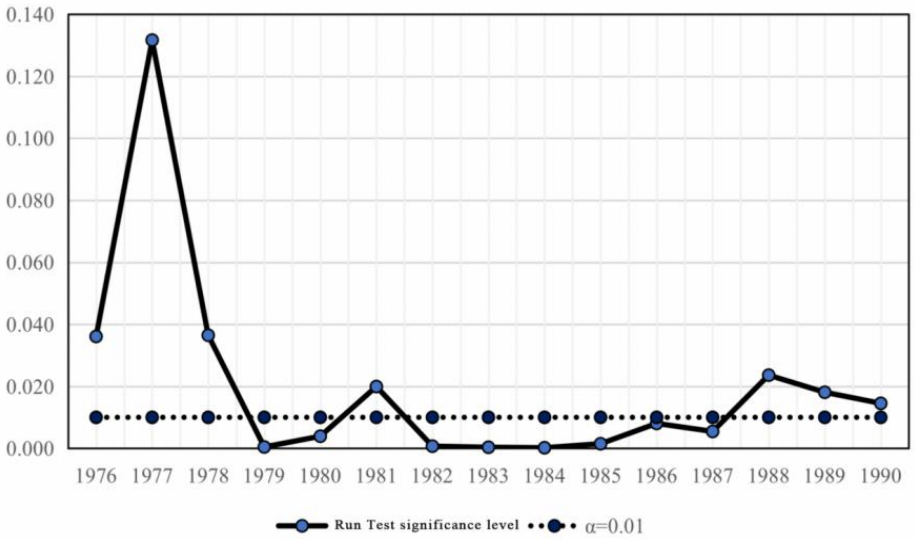

Figure 5. *Significance level from 1976 to 1990 by run test*

Table 2. *Results of Spearman rank correlation test and run test of meteorological elements*

Factor		***RH*** **(%)**	***SH*** **(h)**	***WS*** **(m/s)**	T_{max} **(℃)**	T_{min} **(℃)**
Spearman rank correlation test	Rank correlation coefficient r_s	-0.43	-0.81	-0.92	0.51	0.85
	Statistic *T*	-3.23	-9.54	-16.59	4.07	11.26
Significance level of run test based on 1983 mutation		2.14E-01	1.90E-04	4.86E-11	1.00	2.52E-03

http://www.aloki.hu ● ISSN 1589 1623 (Print) ● ISSN 1785 0037 (Online)
DOI: http://dx.doi.org/10.15666/aeer/2302_18971921

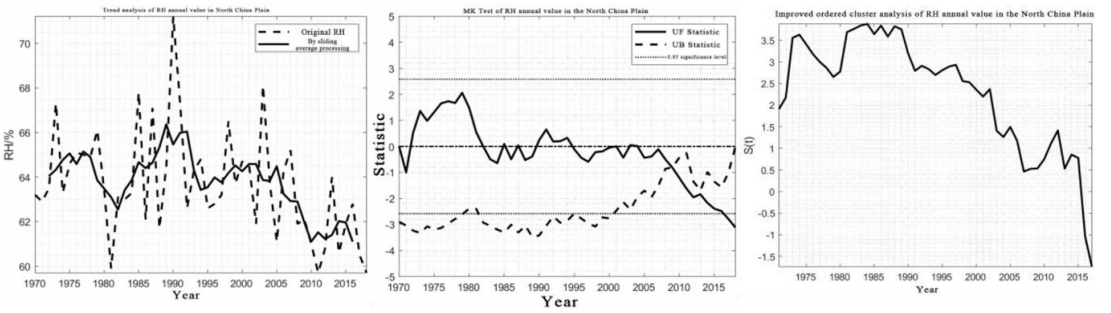

(a) Trend analysis and mutation diagnosis of RH

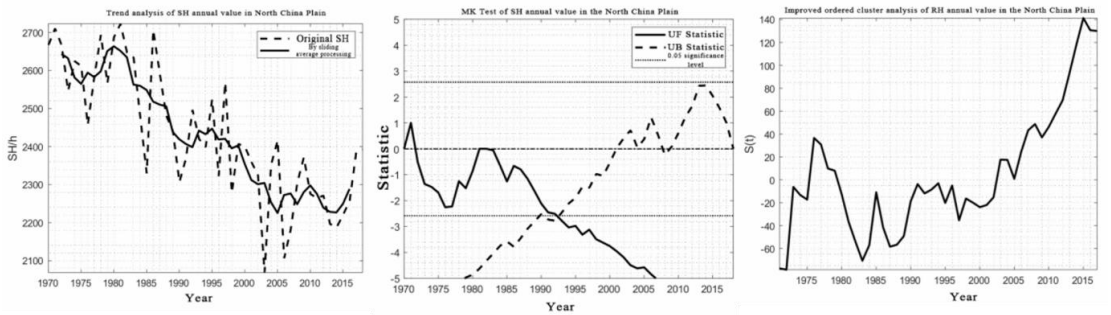

(b) Trend analysis and mutation diagnosis of SH

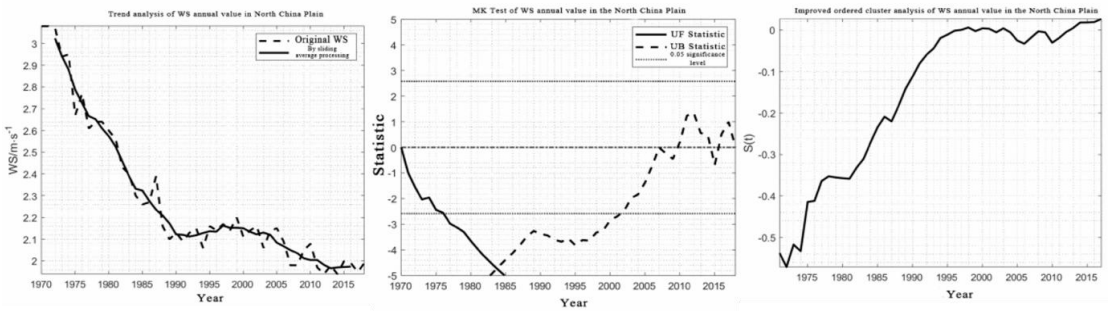

(c) Trend analysis and mutation diagnosis of WS

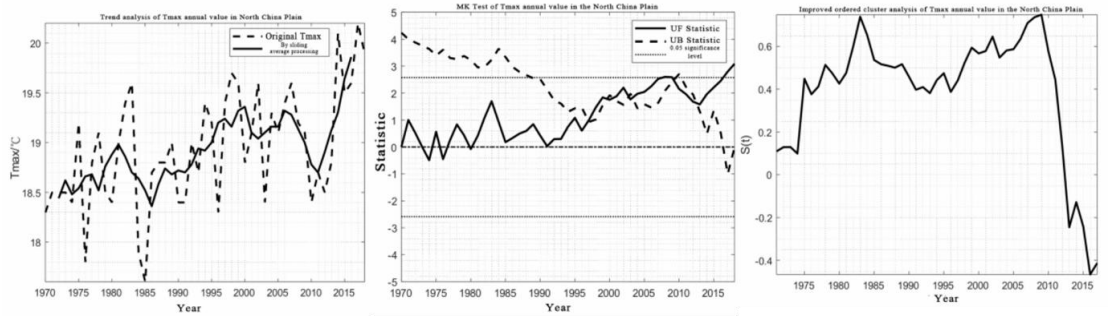

(d) Trend analysis and mutation diagnosis of T_{max}

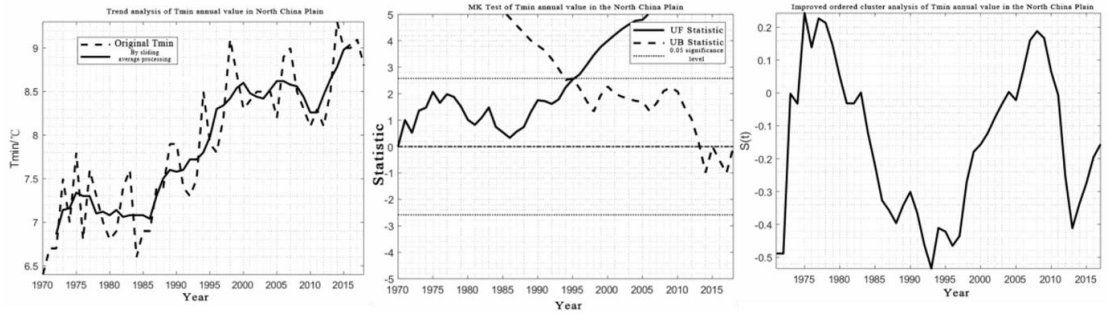

(e) Trend analysis and mutation diagnosis of T_{min}

Figure 6. *Trend analysis and mutation diagnosis of meteorological elements*

http://www.aloki.hu ● ISSN 1589 1623 (Print) ● ISSN 1785 0037 (Online)
DOI: http://dx.doi.org/10.15666/aeer/2302_18971921

Spatial variability of ETo and meteorological elements

Figure 7 reveals the annual reference total evapotranspiration and related climate parameters during 1970-2019. As shown in *Figure 7*, the following conclusions can be reached:

(1) For ETo, the high value range (1085~1039 mm/year) appeared in the west and south of the Bohai Sea area, including most of Tianjin, a small segment of Hebei Province and the Bohai Sea belt of Shandong Province. Compared with high value areas, the northern area near the Bohai Sea, such as Tangshan, Hebei Province, has a relatively low value area (909-997 mm/year). Above results are similar to Zhang et al. (2019), and this paper further refined the differentiation range of ETo. As a whole, the low-value part is easy to appear in the northern and northwestern boundaries of the plain, showing a more obvious hierarchical distinction from the Bohai Sea to the inland boundary.

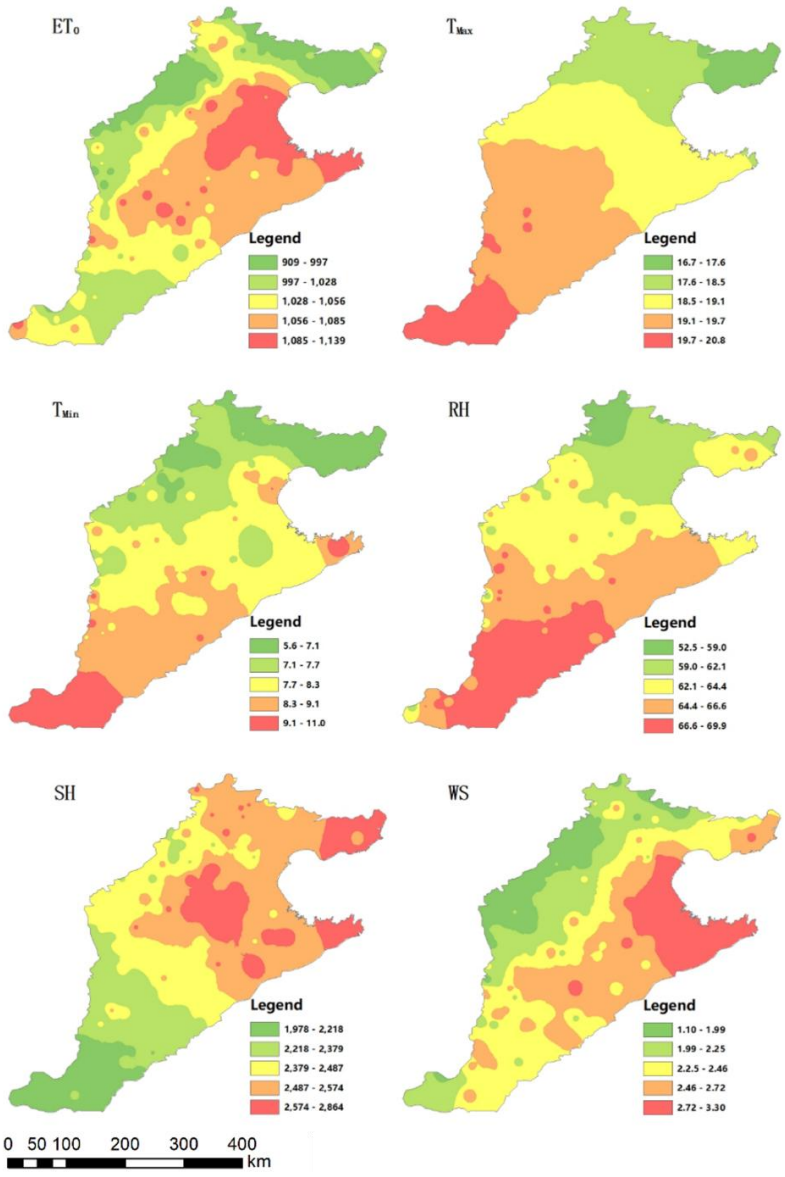

Figure 7. *Average annual value (between 1970 to 2019) of ETo and relative meteorological factors. (The average variation of each element is shown in Fig. 6)*

http://www.aloki.hu ● ISSN 1589 1623 (Print) ● ISSN 1785 0037 (Online)
DOI: http://dx.doi.org/10.15666/aeer/2302_18971921

(2) T_{min} and T_{max} show a north-south gradient from high to low. In particular, the mean minimum temperature in Shandong Province near the Bohai Sea zone is at a higher level than that in North China Plain. RH showed a north-south gradient from high to low, but in the northern part of the Bohai Rim, RH remained at a moderate level. SH decreased from northeast to southwest in the Bohai Rim, and its higher value appeared in the Bohai Rim and the middle part of the whole plain. The long-term WS decreased from southeast to northwest from the southern part of the Bohai Rim.

(3) From the distribution of the 6 subgraphs, the spatial distribution of WS is similar to that of ETo. It is preliminarily and qualitatively considered that WS is an important factor affecting the spatial distribution of ETo in the study plain.

Sensitivity analysis and spatial relationship of ETo and related meteorological elements

First, Pearson correlation coefficient between ETo of each meteorological station and each meteorological element was calculated, and then IDW method was used to obtain grid distribution diagram. *Figure 8* indicates the correlation results. In the distribution diagram of correlation coefficient between ETo and T_{max}, the range is 0.767-0.854, showing a good correlation, with high values appearing in the west and south of North China Plain. In the distribution diagram of ETo and T_{min}, the correlation range is 0.662~0.757, and the correlation is different from the maximum temperature. The high values appear in the north-central and eastern parts, and has the opposite trend with the distribution diagram of the maximum temperature correlation coefficient. The correlation coefficients between *SH* and ETo were concentrated in a small range of 0.506~ 0.654, and showed a decreasing trend from north to south. *RH* was negatively correlated with ETo, and the absolute values were between 0.013 and 0.320. *WS* also has a small impact, and the correlation coefficient locates in 0.140~0.444, with higher value appearing in the central and eastern parts.

Eto is often influenced by a combination of a range of climate parameters. Therefore, OLS model and GWR model should be further used to evaluate the overall correlation between ETo and various climate parameters. For the fitting value of the regression model, statistical indicators corresponding to *Equations 22* and *23* were used.

In order to not lose generality, OLS regression was conducted for annual and monthly ETo from July to September. Among them, the correlation coefficients R2 obtained by OLS model for July-September and annual scale simulation were 0.932, 0.888, 0.929 and 0.927, respectively, and the statistical indicators ranged from 0.019 to 0.027 mm/day (MAE) and 0.537 to 0.768% (MRE). It is preliminarily concluded that OLS model is reliable to simulate annual mean ETo and monthly ETo for our study area. *Table 3* records the difference between the model correlation coefficient obtained after the removal of a single meteorological factor in turn and the original correlation coefficient of the input of all factors. The difference is used to judge the importance order of each factor for different time scales. It can be seen from *Table 3* that for North China Plain, sunshine duration in July is the most important, while the minimum temperature is the least important. Sunshine duration in August is the most important, and the maximum temperature is the least important. In September, wind speed is the most important, and the maximum temperature is the least important. Throughout the year, wind speed is the most important, and minimum temperature is the least important.

http://www.aloki.hu ● ISSN 1589 1623 (Print) ● ISSN 1785 0037 (Online)
DOI: http://dx.doi.org/10.15666/aeer/2302_18971921

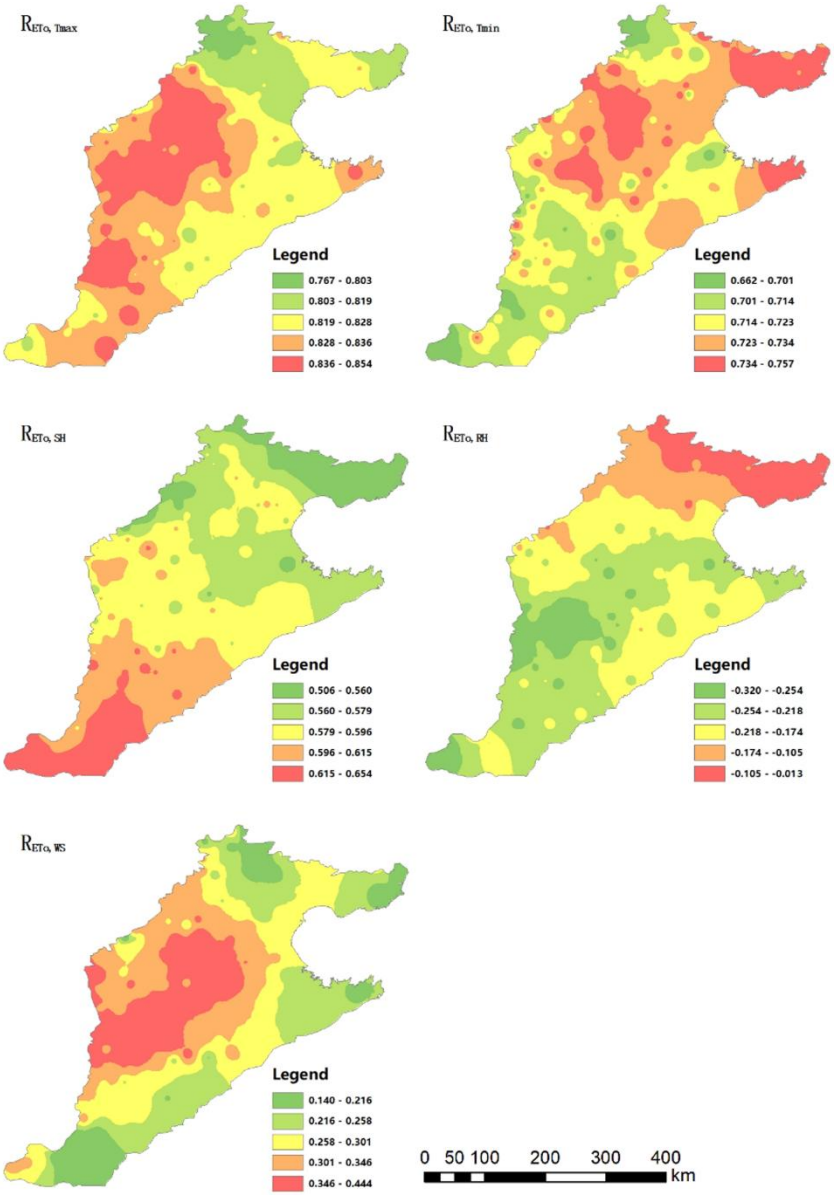

Figure 8. *Correlation coefficients between ETo and meteorological factors*

Table 3. *Differences of correlation coefficient in different time scales after removing relevant meteorological elements based on OLS model*

Elimination of single element	*SH* (*h*)	T_{max} (°C)	*RH* (%)	*WS* (m/s)	T_{min} (°C)
July	0.254	0.035	0.069	0.069	0.012
August	0.248	0.007	0.051	0.033	0.038
September	0.095	0.011	0.031	0.114	0.033
year-round	0.096	0.100	0.120	0.278	0.014

In addition, the geographically weighted regression (GWR) model, as a local regression technique that allows the model parameters to vary with space, is used to

http://www.aloki.hu ● ISSN 1589 1623 (Print) ● ISSN 1785 0037 (Online)
DOI: http://dx.doi.org/10.15666/aeer/2302_18971921

further simulate and analyze the correlation relations in the plain. In this paper, the annual scale ETo regression model is established using GWR4 software. The output of the software contains the local parameter estimation and model diagnosis information of each element of each meteorological station. To identify the difference between GWR and OLS, firstly, GWR regression evaluation results were 0.019 mm/day (MAE) and 0.670% (MRE) respectively, which were very close to the results of OLS model under the same conditions (MAE = 0.019 mm/day, MRE = 0.663%). Secondly, the spatial distribution of residuals between OLS model and GWR model is shown in *Figure 9*.

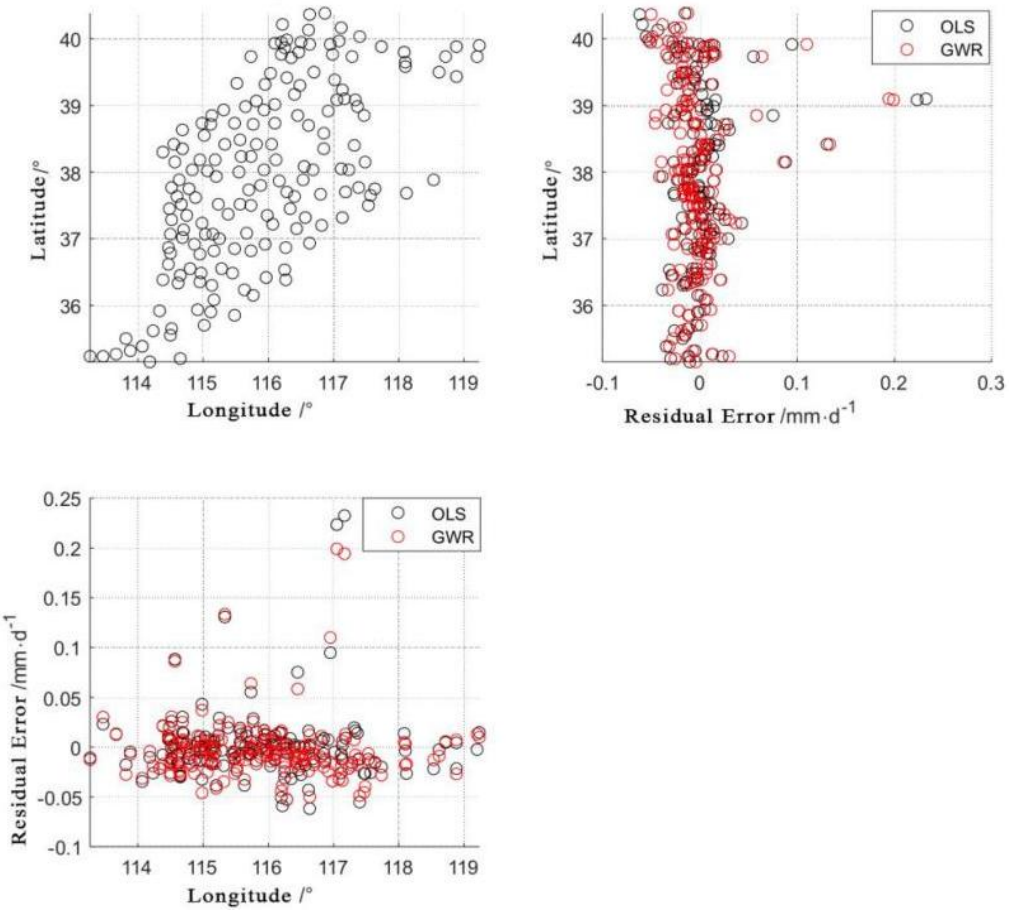

Figure 9. *Spatial distribution of the residual from OLS model and GWR Model at annual scale*

Figure 10 shows the contribution degree of meteorological elements to ETo based on GWR model results and in proportion to the reduction value of local correlation coefficient of a factor.

ETo hotspot analysis

As for the annual variation, *Figure 11* shows the IDW grid diagram of long-term average ETo for each month and the results of cold and hot spots. It is found that the cold and hot spots cluster with statistical significance shows a monthly migration trend.

In addition, turning attention to the interannual distribution, *Figure 12* shows the IDW grid diagram of the average total ETo in North China Plain during 1971-1980, 1981-1990, 1991-2000, 2001-2010, and 2011-2019.

http://www.aloki.hu ● ISSN 1589 1623 (Print) ● ISSN 1785 0037 (Online)
DOI: http://dx.doi.org/10.15666/aeer/2302_18971921

Discussion

Figure 2 shows that the ETo series presents an overall decreasing trend. Since 1970, ETo has been on a downward trend. Although there was a brief upward phase in the late 1970s, the decline range became larger and after the transition in the 1980s, it dropped to a relatively low value in the 1990s. Then there was a small climb to 2000, but the range remained relatively stable. According to the ET sequence from 1970 to 2019, the rank correlation coefficient is r_s = -0.485, and the statistic T = -3.8. Using α = 0.01 significance level corresponds to the interpolation of t distribution table $\alpha/2$ = 2.684, therefore $|T| > t_{\alpha/2}$. Combined with the sign of the rank correlation coefficient r_s and the sliding average results, the ETo sequence in the plain has a significant decreasing trend.

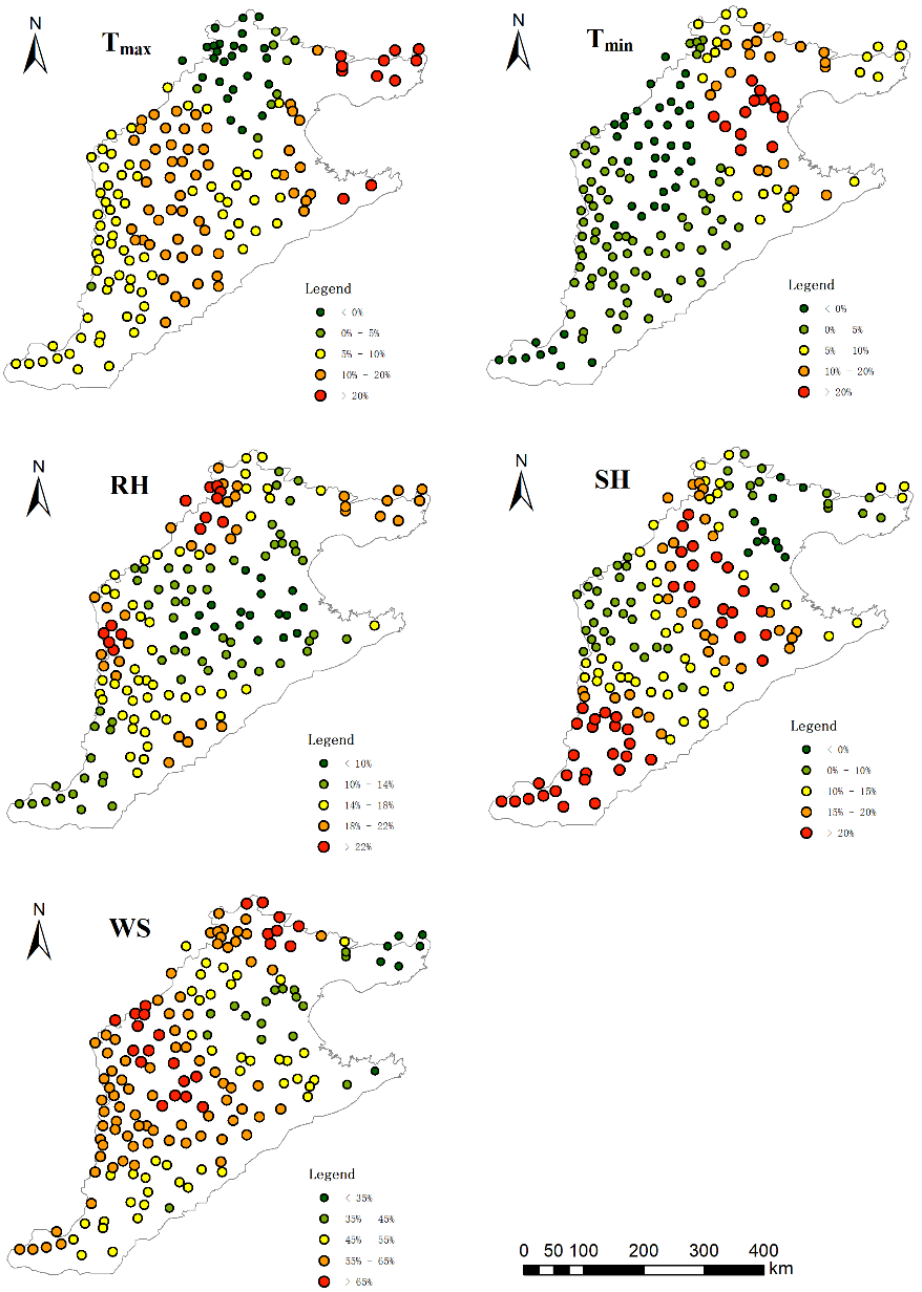

Figure 10. *Contributions of meteorological factors via GWR*

http://www.aloki.hu ● ISSN 1589 1623 (Print) ● ISSN 1785 0037 (Online)
DOI: http://dx.doi.org/10.15666/aeer/2302_18971921

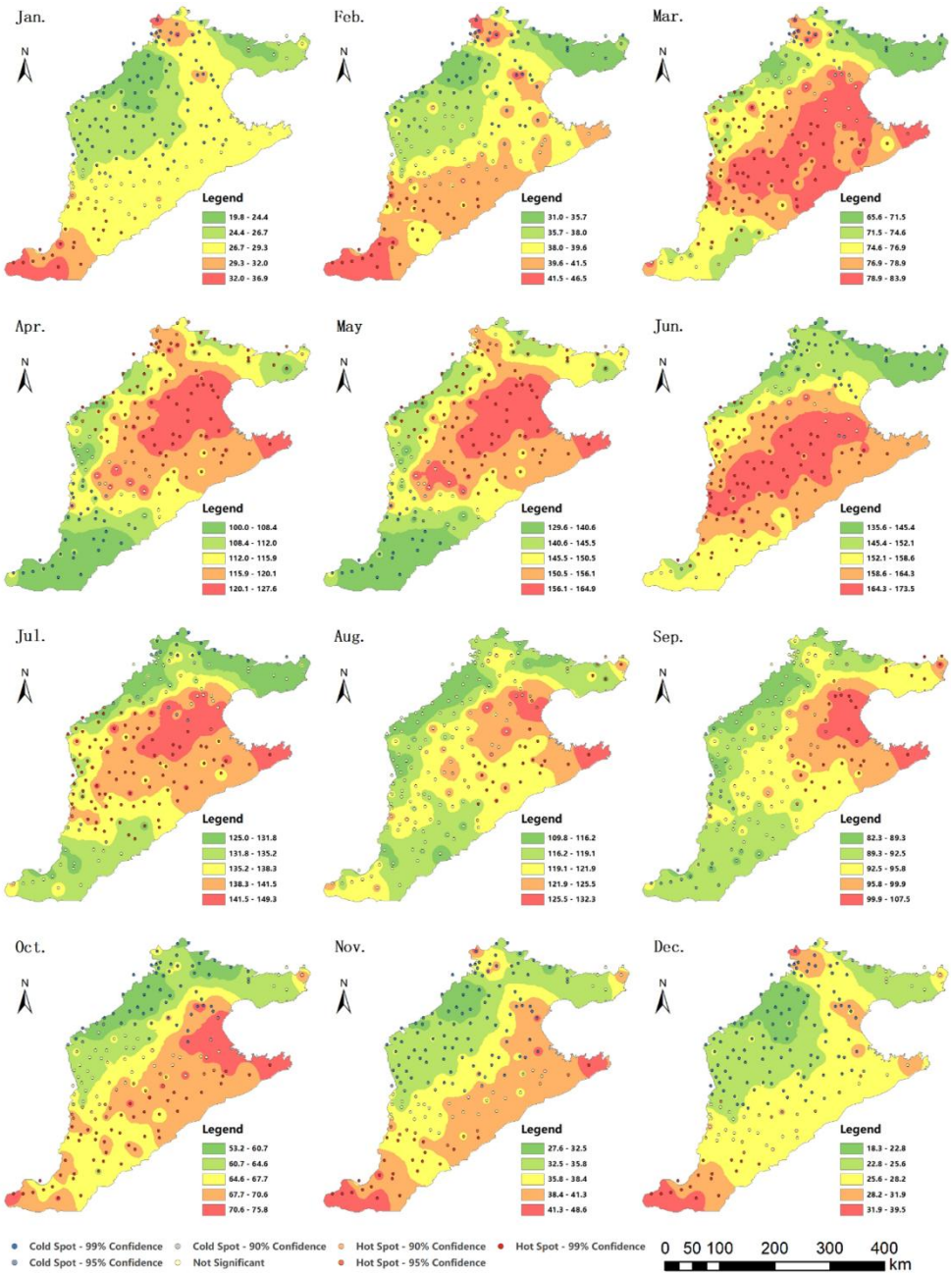

Figure 11. *Hot spot analysis of the monthly reference evapotranspiration in different stages (mm/month)*

The contribution of various meteorological factors (including *RH*, *SH*, *WS*, T_{max} and T_{min}) to the abrupt change of reference crop evaporation in North China Plain in 1983 was discussed. Firstly, Spearman rank correlation test and run test were used to determine the trend of each meteorological element and the significance level of abrupt change in 1983, and the results were recorded in *Table 2*. For Spearman rank correlation test, $\alpha = 0.01$ and $t_{\alpha/2} = 2.684$ were obtained. Therefore, the change trend of all meteorological elements was significant. It is not difficult to see that *SH*, *WS* and T_{min} show the most obvious trend. *SH* and *WS* were decreased while T_{min} was increased. Similarly, the results of run test can be considered that the above three factors had mutations in 1983. The results in *Figure 6* also

http://www.aloki.hu ● ISSN 1589 1623 (Print) ● ISSN 1785 0037 (Online)
DOI: http://dx.doi.org/10.15666/aeer/2302_18971921

verify the above judgment again. Therefore, *SH*, *WS* and T_{min} contributed significantly to the abrupt change of ETo in 1983.

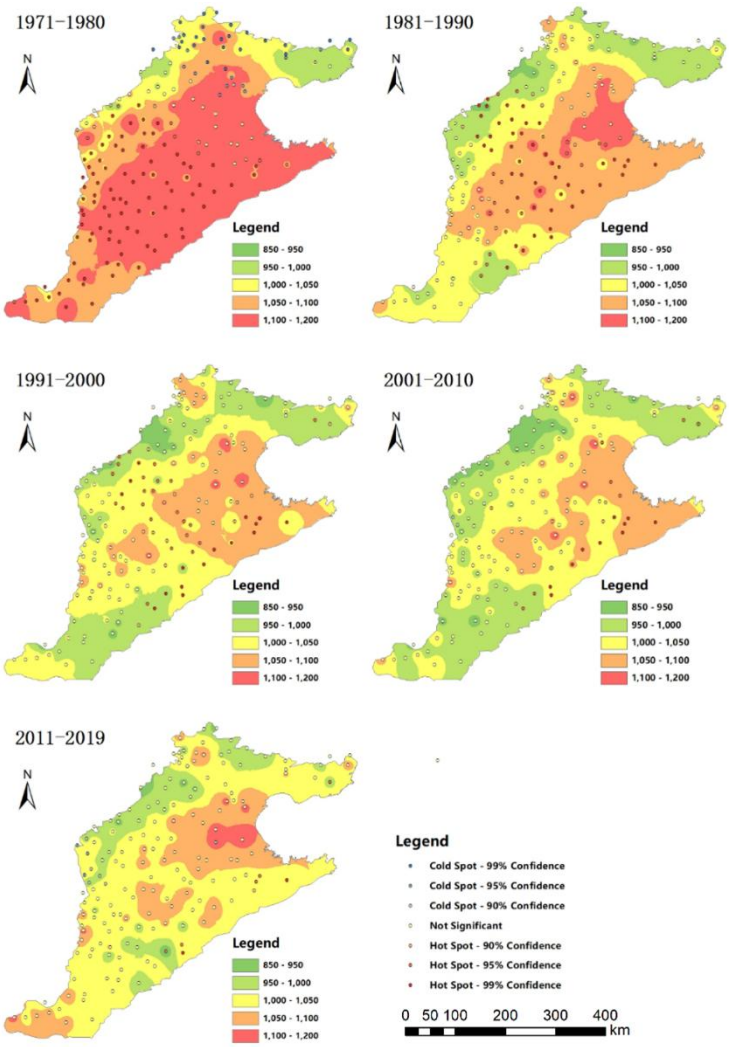

Figure 12. *Hot spot analysis of the yearly reference evapotranspiration in different stages (mm/year)*

As shown in *Figure 7*, the following conclusions can be reached:

(1) For ETo, the high value range (1085~1039 mm/year) appeared in the west and south of the Bohai Sea area, including most of Tianjin, a small segment of Hebei Province and the Bohai Sea belt of Shandong Province. Compared with high value areas, the northern area near the Bohai Sea, such as Tangshan, Hebei Province, has a relatively low value area (909-997 mm/year). Above results are similar to Zhang et al. (2019), and this paper further refined the differentiation range of ETo. As a whole, the low-value part is easy to appear in the northern and northwestern boundaries of the plain, showing a more obvious hierarchical distinction from the Bohai Sea to the inland boundary.

(2) T_{min} and T_{max} show a north-south gradient from high to low. In particular, the mean minimum temperature in Shandong Province near the Bohai Sea zone is at a higher level than that in North China Plain. RH showed a north-south gradient from

http://www.aloki.hu ● ISSN 1589 1623 (Print) ● ISSN 1785 0037 (Online)
DOI: http://dx.doi.org/10.15666/aeer/2302_18971921

high to low, but in the northern part of the Bohai Rim, RH remained at a moderate level. SH decreased from northeast to southwest in the Bohai Rim, and its higher value appeared in the Bohai Rim and the middle part of the whole plain. The long-term WS decreased from southeast to northwest from the southern part of the Bohai Rim.

(3) From the distribution of the 6 subgraphs, the spatial distribution of WS is similar to that of ETo. It is preliminarily and qualitatively considered that WS is an important factor affecting the spatial distribution of ETo in the study plain.

According to *Figure 9*, both models lose their spatial stationarity in the study area, and there are anomalies in the north of the plain and near the Bohai Bay. Compared with the whole data set of 170 sites, the number of outliers is small, which may be due to errors in the basic meteorological data. Finally, after the anomalies were processed, OLS model and GWR model were in line with normal distribution under Kolmogorov-Smirnov test, and the mean values were -0.0052 and -0.0068 respectively, very close to 0. Moreover, there was no significant difference between the residual sequence of the two models by T-test. Both OLS model and GWR model provide reliable performance.

Based on *Figure 10*, the contribution degree of wind speed WS to ETo is the most obvious, which is consistent with the results of annual scale calculation in *Table 3*. Except for WS, the contribution ranges of other factors were similar, but t Tmax, T_{min} and SH had negative contribution levels at a few sites, indicating that the addition of this index factor in these sites affected the accuracy of ETo estimation (as determined by correlation coefficient R2). In the north and south of Bohai Bay, the contribution of Tmax is more obvious, while WS contribution in this area is the lowest compared with other areas, which has the opposite trend to Tmax but is still the dominant factor, and other factors have moderate influence in this area. T_{min} has a small contribution (<5%) over the western and central parts of the area, and a high contribution (<20%) only in the western part of the Bohai Bay. The contribution degree of relative humidity RH is the smallest, and the contribution degree of sunshine duration SH is the highest in the southern part of the plain, along with the middle and northern part. The contribution of WS is relatively high on the whole, and the high value is distributed along the western part of the study plain. This study is slightly different from the conclusion of Zhang et al. (2019), which said the maximum temperature is the main factor affecting ETo in North China Plain. Such differences may be due to differences in data collection, and contribution calculation methods.

According to *Figure 11*, from December to January, hot spots are mainly distributed in the southern tail area of North China Plain, while cold spots occupy most of the range, and no statistically significant spots are distributed on the southeast boundary. February is a transition period, after February, hot spots move north, while cold spots move closer to the border. From March to July, hot spots dominated and cold spots concentrated in the border areas. In August and September, non-statistically significant points accounted for the majority of the hot spots concentrated in the Bohai Rim region. With the arrival of winter, cold spots begin to migrate to most segments of the plain in October to November. As a result, hot spots tend to become areas with high ETo values, which are more prone to water shortages and droughts. For hot spots requiring irrigation, where dry seasons will require more water.

Based on *Figure 12*, the range of annual mean total ETo has not sharply changed in the past 50 years, ranging from 850 mm/year to 1200 mm/year. However, the spatial distribution of ETo has changed greatly. As can be seen from the two subgraphs from 1971-1980 and 1981-1990, the region with high value of ETo experienced drastic

http://www.aloki.hu ● ISSN 1589 1623 (Print) ● ISSN 1785 0037 (Online)
DOI: http://dx.doi.org/10.15666/aeer/2302_18971921

atrophy, and the regions with different value levels showed simultaneous decrease of ETo, which was consistent with the view in Section 5.1.2 that 1983 was the abrupt year of ETo. The results of IDW analysis can detect the location of the ETo aggregation, but fail to give their statistically significance. The analysis results of cold and hot spots of annual ETo were obtained by using Getis-Ord statistics and ArcGIS 10.2, also shown in *Figure 11*. The analysis results of hot and cold spots show that: (1) Hot and cold spots with a high confidence level decreased sharply with the progress of time. Finally, in the period from 2011 to 2019, most of all spots could not be determined to have Significant statistical significance (that is, No Significant points accounted for the majority, which could not guarantee the credibility of their ETo); (2) Through IDW grid, it is found that the hot and cold areas from 1971 to 1980 have a good consistency with the areas with high and low ETo values. With the lapse of time to 2000, the significant cold spot gradually disappeared, but the significant hot spot was still concentrated in the middle of the plain. The results of relevant hot and cold spots can give important information for governors.

Conclusion

This study is mainly organized on the basis of relevant daily scale meteorological data from stations in North China Plain during 1970~2019. Various modeling techniques such as sliding average method, Mann-Kendall test, improved ordered cluster analysis, inverse distance weighted interpolation (IDW), ordinary least squares regression (OLS), geographic weighted regression (GWR) and cold and hot spot analysis were conducted to analyze the spatiotemporal variation of the distribution of ETo and related meteorological elements.

(1) The analysis of the annual average total ETo series in North China Plain shows that the ETo has a significant decreasing trend with 99% confidence; The mutation time that caused this decreasing trend was thought to occur in 1983 with the significance of 3.47E-04. The results of the run test reflect that nearly the whole 1980s (1982-1987) was an important period of ETo mutation for the plain. Moreover, sunshine duration *(SH)*, average wind speed *(WS)* at a height of 2 meters and minimum temperature (T_{min}) significantly contributed to the abrupt change of the overall average ETo in 1983.

(2) IDW was employed to conduct spatial analysis of annual mean ETo and mean of meteorological elements, and it reveals that: *a.* For ETo, the high value range (1085~1039 mm/year) occurs in the western and southern parts of Bohai Bay, including most of Tianjin, a small part of Hebei Province and the Bohai belt near Shandong Province. The northern part of Bohai Bay region of relatively low area (909~997 mm/year). *b.* Relative humidity, minimum and maximum temperature show a north-south gradient from high to low. In the Bohai rim region for radiant point, sunshine duration and wind velocity sunshine time trend declines from northeast to southwest, wind speed from the southern Bohai Bay from the southeast to the northwest radiation decreases in turn. *c.* Judging qualitatively from the spatial distribution of each element, wind speed is the main factor affecting ETo in North China Plain.

(3) Sensitivity analysis of various meteorological elements to ETo based on OLS and GWR: *a.* Taking the scales from July to September and the whole year as an example, OLS model analyzed the influence of meteorological elements on ETo at different time scales. It can be seen that wind speed is the most important factor in September and the whole year, while sunshine duration is the most important factor in July and September.

http://www.aloki.hu ● ISSN 1589 1623 (Print) ● ISSN 1785 0037 (Online)
DOI: http://dx.doi.org/10.15666/aeer/2302_18971921

The minimum temperature is the least influential factor in July and the whole year, and the maximum temperature is the weakest in August and September. However, the spatial distribution of residuals of OLS model and GWR model at the annual scale showed that there were abnormal points. After removing the abnormal points, the residuals simulated by the model were very close to the normal distribution with the mean value of 0, which better guaranteed the spatial stationarity. *b.* The contribution calculation results based on the GWR model further confirm that wind speed is the dominant factor affecting the ETo size, echoing the above qualitative judgment on the influence of mean spatial distribution on wind speed.

(4) The cold and hot spots of ETo distribution in North China Plain were detected with the help of Getis-Ord statistics. *a.* With the change of years, hot spots shrink sharply, especially the gap between 1970s and 1980s is the most obvious, which is strong auxiliary evidence for the diagnosis of mutation mentioned above. From 2011 to 2019, there were no significant ETo hot and cold spots, and the area with high ETo value accounted for a small proportion in the plain. *b.* The annual analysis shows that from December to January, hot spots are mainly distributed in the southern tail area of a small part of the study area, and cold spots occupy most of the area. In February, the hot spot moved northward after the transition period, while the cold spot moved closer to the boundary. Hot spots dominated from March to July, and cold spots were concentrated in the border area in a small range. In August and September, the non-significant points accounted for the main part, and the hot spots concentrated in Bohai Bay. From October to November, the cold spot began to migrate to most parts of the plain. Therefore, hot spots are more likely to be areas with high ETo values.

Finally, the results of this study can help the relevant personnel of water resources planning in North China Plain to better understand the spatial and temporal distribution of regional ETo and meteorological elements, and contribute to the optimal allocation and management of agricultural water resources.

Acknowledgments. This work was financially supported by the Key Science and Technology Program of Henan Province, China (222102110058), State Key Laboratory of Simulation and Regulation of Water Cycle in River Basin, China Institute of Water Resources and Hydropower Research (IWHR-SKL-202104), the National Natural Science Foundation of China, Project No. U2243219 and Outstanding Young Talent Technology Project of Yellow River Conservancy Commission (HQK-202302). We thank the China Scholarship Council for providing the funding.

REFERENCES

[1] Allan, R. G., Pereira, L. S., Raes, D., Smith, M. (1998): Crop evapotranspiration. Guidelines for computing crop water requirements. – FAO Irrigation and Drainage Paper No. 56. FAO, Rome.

[2] Bandyopadhyay, A., Bhadra, A., Raghuwanshi, N. S., Singh, R. (2009): Temporal trends in estimates of reference evapotranspiration over India. – Journal of Hydrologic Engineering 14(5): 508-515. DOI: 10.1061/(ASCE)HE.1943-5584.0000006.

[3] Bo, Z., TiaoFeng, Z. (2013): Response of reference crop evapotranspiration to climate change in the Loess Plateau from 1961 to 2010 and its future trend prediction. – Chinese Journal of Ecology 32(03): 733-740. DOI: 10.13292/j.1000-4890.2013.0113.

[4] Craglia, M., Haining, R., Wiles, P. (2000): A comparative evaluation of approaches to urban crime pattern analysis. – Urban Studies 37(4): 711-729. DOI: 10.1080/00420980050003982.

http://www.aloki.hu ● ISSN 1589 1623 (Print) ● ISSN 1785 0037 (Online)
DOI: http://dx.doi.org/10.15666/aeer/2302_18971921

[5] Dinpashoh, Y., Jhajharia, D., Fakheri-Fard, A., Singh, V. P., Kahya, E. (2011): Trends in reference crop evapotranspiration over Iran. – Journal of Hydrology 399(3): 422-433. DOI: https://doi.org/10.1016/j.jhydrol.2011.01.021.

[6] Duan, Y., Yang, S., Yang, T., Hu, X. (2015): Analysis on long-term change trend of reference crop evapotranspiration in Nantong City. – Hydropower Energy Science 33(02): 19-21. DOI: https://kns.cnki.net/kcms2/article/abstract?v=JTjHPEokuYSRmK-hD__1OeR1EYfzwzXfFh_0-eicWtB_iL47zJYSETyvbSoOxdjfC8pfzBcRXpv_ipOmyUWRWjWFno5qNvhTPPiWtvwIBrTVUqtVePTuA4PEVw6aEkfwI3-t5hTXeJ5P2B5yJCHrWw==&uniplatform=NZKPT&language=CHS.

[7] Gajović, V., Todorovic, B. (2013): Spatial and temporal analysis of fires in Serbia for period 2000-2013. – Journal of the Geographical Institute Jovan Cvijic SASA 63: 297-312. DOI: 10.2298/IJGI1303297G.

[8] Ge, J., Zhao, L., Yu, Z., Liu, H., Zhang, L., Gong, X., Sun, H. (2022). Prediction of Greenhouse Tomato Crop Evapotranspiration Using XGBoost Machine Learning Model. – Plants 11: 1923.

[9] George, H. H. (1975): Moisture availability and crop production. – Transactions of the ASAE 18(5): 980-0984. DOI: https://doi.org/10.13031/2013.36722.

[10] Hao, Z., An, G., Wang, J., Ju, Q., Li, Y. (2013): Trends and causes of reference crop evapotranspiration in the middle and upper reaches of Huaihe River. – Ecology and Environmental Sciences 22(09): 1528-1533. DOI: 10.16258/j.cnki.1674-5906.2013.09.012.

[11] He, C., Wang, Y.-Q., Yu, W.-B., Kou, Y.-H., Yves, B. N. d., Zhao, X., Zhang, H.-L. (2022): Comprehensive analysis of resource utilization efficiency under different tillage systems in North China Plain. – Journal of Cleaner Production 347: 131289. DOI: https://doi.org/10.1016/j.jclepro.2022.131289.

[12] Hu, Y., Liang, Z., Weiming, Z., Xiaowei, L. (2014): Analysis of inconsistent hydrological frequency based on skip diagnosis. – Yellow River 36(06): 51-53+57.

[13] Jensen Marvin, E., Haise Howard, R. (1963): Estimating evapotranspiration from solar radiation. – Journal of the Irrigation and Drainage Division 89(4): 15-41. DOI: 10.1061/JRCEA4.0000287.

[14] Koch, J., Zhang, W., Martinsen, G., He, X., Stisen, S. (2020): Estimating net irrigation across the North China Plain through dual modeling of evapotranspiration. – Water Resources Research 56(12): e2020WR027413. DOI: https://doi.org/10.1029/2020WR027413.

[15] Li, H., Liu, H., Zhijun, Z. (2017): Change trend and influencing factors of reference crop evapotranspiration in Fenhe irrigation area. – Journal of Irrigation and Drainage 36(11): 86-93. DOI: 10.13522/j.cnki.ggps.2017.11.015.

[16] Liu, B., Liu, M., Cui, Y., Shao, D., Mao, Z., Zhang, L., Khan, S., Luo, Y. (2020). Assessing forecasting performance of daily reference evapotranspiration using public weather forecast and numerical weather prediction. – Journal of Hydrology 590:125547.

[17] Lv, L., Liu, X., Zhou, H., Wu, L. (2013): Analysis of annual runoff variation trend in the middle and lower reaches of Yarlung Zangbo River. – Yellow River 35(05): 27-29.

[18] Pour, S. H., Wahab, A. K. A., Shahid, S., Ismail, Z. B. (2020): Changes in reference evapotranspiration and its driving factors in peninsular Malaysia. – Atmospheric Research 246: 105096. DOI: https://doi.org/10.1016/j.atmosres.2020.105096.

[19] Priestley, C. H. B., Taylor, R. J. (1972): On the assessment of surface heat flux and evaporation using large-scale parameters. – Monthly Weather Review 100(2): 81-92. DOI: https://doi.org/10.1175/1520-0493(1972)100<0081:OTAOSH>2.3.CO;2.

[20] Songchitruksa, P., Zeng, X. (2010): Getis–Ord spatial statistics to identify hot spots by using incident management data. – Transportation Research Record 2165(1): 42-51. DOI: 10.3141/2165-05.

http://www.aloki.hu ● ISSN 1589 1623 (Print) ● ISSN 1785 0037 (Online)
DOI: http://dx.doi.org/10.15666/aeer/2302_18971921

[21] Srivastava, N., Rao, V., Korwar, G., Venkateswarlu, B. (2010): Micro-level spatial variability and temporal trends in reference evapotranspiration (ETo) at a semi-arid tropical station. – Journal of Agrometeorology 12: 208-212. DOI: 10.54386/jam.v12i2.1307.
[22] Tabari, H., Aeini, A., Talaee, P. H., Somee, B. S. (2012): Spatial distribution and temporal variation of reference evapotranspiration in arid and semi-arid regions of Iran. – Hydrological Processes 26(4): 500-512. DOI: https://doi.org/10.1002/hyp.8146.
[23] Turc, L. (1961): Estimation of irrigation water requirements, potential evapotranspiration: a simple climatic formula evolved up to date. – Annales Agronomiques 12: 13-49
[24] Wolf, T., McGregor, G. (2013): The development of a heat wave vulnerability index for London, United Kingdom. – Weather and Climate Extremes 1: 59-68. DOI: https://doi.org/10.1016/j.wace.2013.07.004.
[25] Yang, G., Li, S., Wang, H., Wang, L. (2022): Study on agricultural cultivation development layout based on the matching characteristic of water and land resources in North China Plain. – Agricultural Water Management 259: 107272. DOI: https://doi.org/10.1016/j.agwat.2021.107272.
[26] Yuan, M., Wang, W., Binlin, Y. (2017): The improvement of ordered clustering analysis Method and its application to the identification of abrupt points in hydrological series. – Chinese Journal of Hydrology 37(05): 8-11.
[27] Zhang, L., Cui, Y., Xiang, Z., Zheng, S., Traore, S., Luo, Y. (2018): Short-term forecasting of daily crop evapotranspiration using the 'Kc-ETo' approach and public weather forecasts. – Archives of Agronomy and Soil Science 64(7): 903-915. DOI: 10.1080/03650340.2017.1387778.
[28] Zhang, L., Traore, S., Cui, Y., Luo, Y., Zhu, G., Liu, B., Fipps, G., Karthikeyan, R., Singh, V. (2019): Assessment of spatiotemporal variability of reference evapotranspiration and controlling climate factors over decades in China using geospatial techniques. – Agricultural Water Management 213: 499-511. DOI: https://doi.org/10.1016/j.agwat.2018.09.037.
[29] Zhang, L., Zhao, X., Ge, J., Zhang, J., Traore, S., Fipps, G., Luo, Y. (2022a): Evaluation of Five Equations for Short-Term Reference Evapotranspiration Forecasting Using Public Temperature Forecasts for North China Plain. – Water. DOI: 10.3390/w14182888.
[30] Zhang, L., Zhang, J., Traore, S., Ge, J., Zhao, X., Zhan, H., Singh, V. P. (2022b). Continental-scale spatiotemporal calibration of the Blaney–Criddle equation for different climate zones in China. – Journal of Hydrology: Regional Studies 44: 101233.
[31] Zhang, L., Zhao, X., Zhu, G., He, J., Chen, J., Chen, Z., Traore, S., Liu, J., Singh, V. P. (2023). Short-term daily reference evapotranspiration forecasting using temperature-based deep learning models in different climate zones in China. – Agricultural Water Management 289: 108498.
[32] Zhang, X., Yang, M., Jifeng, L. (2020): Abrupt point diagnosis of transits in Inner Mongolia reach of the Yellow River. – Yellow River 42(S2): 21-22+33.
[33] Zhang, Z., Lin, A., Zhao, L., Zhao, B. (2022c): Attribution of local land surface temperature variations response to irrigation over the North China Plain. – Science of the Total Environment 826: 154104. DOI: https://doi.org/10.1016/j.scitotenv.2022.154104.
[34] Zhao, X., Zhang, L., Zhu, G., Cheng, C., He, J., Traore, S., Singh, V. P. (2023). Exploring interpretable and non-interpretable machine learning models for estimating winter wheat evapotranspiration using particle swarm optimization with limited climatic data. – Computers and Electronics in Agriculture 212: 108140.

http://www.aloki.hu ● ISSN 1589 1623 (Print) ● ISSN 1785 0037 (Online)
DOI: http://dx.doi.org/10.15666/aeer/2302_18971921